

# $^{52}\text{Cr}$ Spinor Condensate— A Biaxial or Uniaxial Spin Nematic

Roberto B. Diener and Tin-Lun Ho

Department of Physics, The Ohio State University, Columbus, OH

(Dated: November 9, 2018)

We show that the newly discovered  $^{52}\text{Cr}$  Bose condensate in zero magnetic field can be a spin nematic of the following kind: A “maximum” polar state, a “co-linear” polar state, or a biaxial nematic ferromagnetic state. We also present the phase diagram with a magnetic field in the interaction subspace containing the Chromium condensate. It contains many uniaxial and biaxial spin nematic phases, which often but not always break time reversal symmetry, and can exist with or without spontaneous magnetization.

Recently, Tilman Pfau’s group at Stuttgart has succeeded in condensing a Bose gas of  $^{52}\text{Cr}$ [1].  $^{52}\text{Cr}$  atoms are spin-3 bosons with electronic spin  $J = 3$  and nuclear spin  $I = 0$ . In contrast, alkali bosons such as  $^{87}\text{Rb}$  and  $^{23}\text{Na}$  are spin-1 or -2 bosons with  $J = 1/2$  and  $I = 3/2$ . Since  $^{52}\text{Cr}$  has a  $J$  6 times larger than the alkali’s, its dipolar interaction is 36 times larger. Indeed, dipolar effects have been observed in Cr[2], although they have not been observed in the alkalis. For this reason, Cr is sometimes referred to as a “dipolar condensate. This characterization is not quite appropriate. Despite their observability, the dipolar energy is no more than a few percent of the total energy. As we shall see, if the spin degrees of freedom of Cr is released, it will have many remarkable spin nematic structures stabilized by energies much larger than the dipole energy. The Cr condensate, in short, is a quantum spin nematic.

At present, experiments on  $^{52}\text{Cr}$  are performed in magnetic traps which freeze the atomic spins. The spin degrees of freedom, however, can be released in optical traps. In the case of optically trapped  $^{87}\text{Rb}$  and  $^{23}\text{Na}$ , ground states of different magnetic structures have been discovered. Since Cr atoms have a higher spin, the number of possible phases will increase. Cr also differs from the alkalis in that its scattering lengths in different angular momentum channels are very different, whereas they are very similar in the alkalis. According to ref.[3], the closer these scattering lengths, the weaker the spin-dependent interactions. Thus the ratio between spin-dependent and density-density interactions in the alkalis is about 1% while it is of order 1 in  $^{52}\text{Cr}$ . In other words, once the spins of Cr are unfrozen, *the spin-dependent interactions will overwhelm the dipole energy*. Any novel properties of Cr spinor BEC will be consequences of the spin interaction with dipolar effects as a perturbation.

For spin-3 bosons, the interactions are specified by the scattering lengths  $a_S$  in total angular momentum channel  $S = 0, 2, 4, 6$ . At present, all  $a_S$  except  $a_0$  have been determined[2]. The physical system therefore lies on a line in the interaction parameter space, which we refer to as the “Cr”-line. While we shall focus on this line, we also present the phase diagram as a function of interaction and magnetic field, for it will be useful for other spin-3 Bose systems. As we shall see, the phase diagram is full of

spin nematic phases which are either uniaxial or biaxial. These phases typically but not always break time reversal symmetry, which can come about with and without a spontaneous magnetization [4]. The discovery of some of these nematic phases will be exciting indeed.

**I. The spin-dependent energy functional:** Let  $\Psi_m = \sqrt{n} \zeta_m$ ,  $m = -3$  to  $3$ , be the condensate of a spin-3 Bose gas, where  $n$  is the density, and  $\zeta^\dagger \zeta = 1$ . As shown in ref.[3], the ground state of a homogenous or single mode spinor condensate in zero magnetic field is determined by the energy  $E/E_o = \sum_{S=0,2,4,6} \tilde{a}_S \mathcal{P}_S$ ,  $\tilde{a}_S = a_S/a_B$ , where  $E_o = \int (2\pi\hbar^2 a_B/M)n^2$ ,  $a_B$  is the Bohr radius,  $\mathcal{P}_S = \sum_{M=-S}^S |B_{S,M}|^2$ , and  $B_{S,M} = \sum_{m,m'} \zeta_m \zeta_{m'} \langle S, M | 3, m; 3, m' \rangle$  is the amplitude of forming a boson pair in state state  $|S, M\rangle$ . In the case of spin-1 alkali gases, (where  $S = 0, 2$  in the energy  $E$ ), the  $a_S$ ’s differ from each other only by about a few percent, so  $E$  is almost an identity. In contrast,  $^{52}\text{Cr}$  has  $a_2 = -7a_B$ ,  $a_4 = 58a_B$ ,  $a_6 = 112a_B$ , while  $a_0$  is undermined[2]. Using the method in ref. [3],  $E$  can be written as[5]

$$E = E_o \left[ \alpha |\Theta|^2 + \beta \sum_{M=-2}^2 |B_M|^2 + \gamma \langle \mathbf{S} \rangle \cdot \langle \mathbf{S} \rangle + C \right] \quad (1)$$

where  $\langle \mathbf{S} \rangle = \zeta_m^* \mathbf{S}_{mm'} \zeta_{m'}$ ,  $B_M = \sqrt{7} B_{2,M}$ ,  $\Theta = \sqrt{7} B_{0,0}$ , so that  $\mathcal{P}_2 = 7 \sum_M |B_M|^2$  and  $\mathcal{P}_0 = 7 |\Theta|^2$ . The coefficients are defined as  $\alpha = \frac{1}{7a_B} [(a_0 - a_6) + \frac{21}{11}(a_6 - a_4)]$ ,  $\beta = \frac{1}{7a_B} [(a_2 - a_6) + \frac{18}{11}(a_6 - a_4)]$ ,  $\gamma = \frac{1}{11a_B}(a_6 - a_4)$ , and  $C = \frac{1}{7a_B} [a_6 - \frac{9}{11}(a_6 - a_4)]$ . We then have  $\beta = -4.38$ ,  $\gamma = 4.91$ ,  $C = 67.8$ , and  $\alpha$  undetermined. Using the relation between  $\mathbf{S}_1 \cdot \mathbf{S}_2$ ,  $(\mathbf{S}_1 \cdot \mathbf{S}_2)^2$  and the projection operators  $P_i$ [6], we can further express eq.(1) in terms of the nematic tensor  $\mathcal{N}_{ij} \equiv \langle (S_i S_j + S_j S_i) \rangle / 2$  as

$$E/E_o = \bar{\alpha} |\Theta|^2 + \bar{\beta} \text{Tr} \mathcal{N}^2 + \bar{\gamma} \langle \mathbf{S} \rangle \cdot \langle \mathbf{S} \rangle + \bar{C}, \quad (2)$$

where  $\bar{\alpha} = \alpha - \frac{5}{3}\beta$ ,  $\bar{\beta} = \beta/18$ ,  $\bar{\gamma} = \gamma - \frac{5}{12}\beta$ ,  $\bar{C} = C - 10\beta$ . For Cr, we have  $\bar{\beta} = -4.38$ ,  $\bar{\gamma} = 2.36$ ,  $\bar{C} = 111.56$  and  $\bar{\alpha}$  is unknown.

**II. Dipole energy :** To get an idea of the general structure of  $E_D$ , we use the single mode approximation so that all components of  $\Psi_\mu$  have the same spatial function,  $\Psi_\mu(\mathbf{r}) = \sqrt{n(\mathbf{r})} \zeta_\mu$ , and  $\zeta_\mu$  has no spatial dependence. For harmonic traps  $V_T = \frac{M}{2} \sum_{i=1}^3 \omega_i^2 (\mathbf{r} \cdot \hat{\mathbf{a}}_i)^2$ ,

where  $(\hat{\mathbf{a}}_1, \hat{\mathbf{a}}_2, \hat{\mathbf{a}}_3)$  is an orthonormal triad, the dipole energy is (see footnote [7])

$$E_D/E_o = \sum_{i=1}^3 \eta_i (\langle \mathbf{S} \rangle \cdot \hat{\mathbf{a}}_i)^2, \quad (3)$$

where  $\eta_i = \frac{1}{2E_o} (g\mu_B)^2 \int d\mathbf{r}_1 d\mathbf{r}_2 n(\mathbf{r}_1) n(\mathbf{r}_2) [1 - 3(\hat{\mathbf{a}}_i \cdot \hat{\mathbf{r}})^2]/r^3$ ,  $\mathbf{r} = \mathbf{r}_1 - \mathbf{r}_2$ . In particular, we denote the direction with smallest  $\eta$  as  $\hat{\mathbf{a}}_3$ . Combining the  $\gamma$  term in eq.(1) with eq.(3), all  $\langle \mathbf{S} \rangle$ -dependent terms in the energy can be written as in eq.(3) with  $\eta_i \rightarrow \eta_i + \gamma$ . The effect of the dipole energy is to align  $\langle \mathbf{S} \rangle$  along the direction  $\hat{\mathbf{a}}_3$ . The phase diagram in zero magnetic field including dipole energy can therefore be obtained by first minimizing eq.(1) (without dipole energy), then replace  $\gamma$  by  $\gamma - \eta_3$ , and align the spontaneous magnetization of those phases that acquire it along  $\hat{\mathbf{a}}_3$ .

To estimate the magnitude of  $\eta_i$ , it is straightforward to show that  $\eta_i = \frac{-(g\mu_B)^2}{4\pi\hbar^2 a_B/M} \frac{4\pi I_i}{3} = -1.7I_i$  where  $I_i = \int_{\mathbf{q}} |n(\mathbf{q})|^2 (1 - 3(\hat{\mathbf{a}}_i \cdot \hat{\mathbf{q}})^2) / \int_{\mathbf{q}} |n(\mathbf{q})|^2$ . Approximating  $n(\mathbf{r})$  as a Gaussian so that  $n(\mathbf{q}) = C e^{-\sum_{i=1}^3 q_i^2 R_i^2}$ , where  $R_i$  is the radius of the atom cloud along  $\hat{\mathbf{a}}_i$  and for cylindrical traps ( $R_x = R_y = R_{\perp} \neq R_z$ ),  $I_z$  varies from 0 to 0.7 as  $R_z/R_{\perp}$  varies from 1 to 10. Thus,  $\eta_i$  is at most about 25% of  $\gamma$ . As we shall see, all the phases along the Cr-line either have zero magnetization, or a weak spontaneous magnetization such that the  $\gamma$  term in eq.(1) contributes very little to the total energy. Since  $E_D$  is dominated by the  $\gamma$  term, it can be ignored as a first approximation.

**III. Relation between singlet amplitude  $\Theta$ , magnetization  $\langle \mathbf{S} \rangle$ , and the nematic tensor  $\mathcal{N}$ :** The quantities  $\Theta$ ,  $\langle \mathbf{S} \rangle$ , and  $\mathcal{N}$  provide a characterization of the phases. They are, however, not independent quantities. Let us first consider  $\Theta$ , which is  $\Theta = 2\zeta_3\zeta_{-3} - 2\zeta_2\zeta_{-2} + 2\zeta_1\zeta_{-1} - \zeta_0^2 \equiv A_{mm'}^{(o)} \zeta_m \zeta_{m'}$ , where  $A_{mm'}^{(o)} = (-1)^{m+1} \delta_{m+m',0}$  is the matrix for spin change under time reversal. It is also easy to show that the maximum value of  $|\Theta|^2$  is 1, and the condition for this is that  $\zeta$  is invariant (up to a phase  $\chi$ ) under time reversal, i.e.  $(A^{(o)}\zeta)_m^* = e^{i\chi} \zeta_m$ . This also implies  $\langle \mathbf{S} \rangle = 0$  [8]. Thus *any state with  $|\Theta| < 1$  breaks time reversal symmetry*.

In the presence of a magnetic field  $\mathbf{B} = B\hat{\mathbf{z}}$ , the rotational invariance of eq.(1) implies that

$$E/E_o = \alpha|\Theta|^2 + \beta \sum_{M=-2}^2 |B_M|^2 + \gamma \langle \mathbf{S} \rangle^2 - p \langle S_z \rangle + C, \quad (4)$$

where  $p = g\mu_B B/E_o$ . Next, we note that the tensor  $\mathcal{N}$  is hermitian. It then has the diagonal form  $\mathcal{N}_{ij} = \lambda_1 \hat{\mathbf{e}}_{1i} \hat{\mathbf{e}}_{1j} + \lambda_2 \hat{\mathbf{e}}_{2i} \hat{\mathbf{e}}_{2j} + \lambda_3 \hat{\mathbf{e}}_{3i} \hat{\mathbf{e}}_{3j}$ , where  $\{\hat{\mathbf{e}}_a\}$  are the principal axes, ( $a = 1, 2, 3$ ),  $\hat{\mathbf{e}}_a \cdot \hat{\mathbf{e}}_b = \delta_{ab}$ , and the  $\lambda_a = \langle (\hat{\mathbf{e}}_a \cdot \mathbf{S})^2 \rangle > 0$  are the eigenvalues, satisfying

$$\lambda_1 + \lambda_2 + \lambda_3 = S(S+1) = 12, \quad S = 3. \quad (5)$$

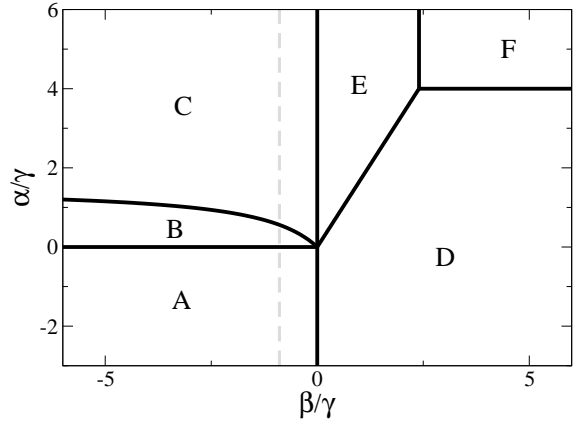


FIG. 1: Phase diagram in zero magnetic field for  $\gamma > 0$ . The dashed line (referred to as the “Cr”-line) is where the physical system lies. The solid lines are first order boundaries. The nature of the phases displayed are discussed in Fig. 3.

We shall order the  $\lambda$ 's so that  $\lambda_1 \leq \lambda_2 \leq \lambda_3$ . The axes  $(\hat{\mathbf{e}}_1, \hat{\mathbf{e}}_2, \hat{\mathbf{e}}_3)$  will be referred to as minor, middle, and major axis respectively. Without loss of generality, we can always arrange  $(\hat{\mathbf{e}}_1, \hat{\mathbf{e}}_2, \hat{\mathbf{e}}_3)$  in a right handed triad. Using the terminology of liquid crystals, the system is referred as a (spin) nematic if  $\mathcal{N}$  is not isotropic, i.e. not proportional to the identity matrix. Systems with two identical eigenvalues and three unequal eigenvalues will be referred to as uniaxial and biaxial nematics respectively.

The origin of different phases is due the competition of  $\Theta$ ,  $\langle \mathbf{S} \rangle$ , and  $\mathcal{N}$ , which are not independent quantities. Such competition can be illustrated by considering  $\bar{\beta} < 0$ , in which case  $\text{Tr} \mathcal{N}^2$  in eq.(2) favors  $\lambda_3 = 9$ ,  $\lambda_1 = \lambda_2 = 3/2$ , which can be achieved by either the polar state  $(1, 0, 0, 0, 0, 0, 1)/\sqrt{2}$ , or the ferromagnetic state  $(1, 0, 0, 0, 0, 0, 0)$ . However, neither of these states are favored simultaneously by the  $\Theta$  term when  $\bar{\alpha} > 0$ , and the  $\langle \mathbf{S} \rangle^2$  term, since  $\bar{\gamma} > 0$  for Cr. One of the key features we find below is that magnetization (be it spontaneous or induced) is generally accompanied with biaxial nematicity. Even though the energy functional is rotationally symmetric about the external field  $\hat{\mathbf{z}}$ , this symmetry is broken spontaneously in the biaxial nematic state.

**IV. Phase diagram in zero magnetic field,  $p = 0$ :** We have minimized eq.(1) by a combination of analytic and numerical methods. The phase diagrams are shown in fig.1 and 2. Since  $\alpha$  is unknown for  $^{52}\text{Cr}$ , the physical system lies on the dotted straight line (or “Cr”-line for short) in fig.1,  $\beta/\gamma = -0.892$ . It passes through the phases A, B, and C, which we name “maximum polar” state (A), co-linear polar state (B), and biaxial nematic ferromagnetic state (C), respectively. All order parameters  $\zeta$  displayed below are unique up to a phase factor and an arbitrary spin rotation.

*Symbols and notations:* We characterize each phase by its condensate wavefunction  $\zeta$ , singlet amplitude  $\Theta$ ,

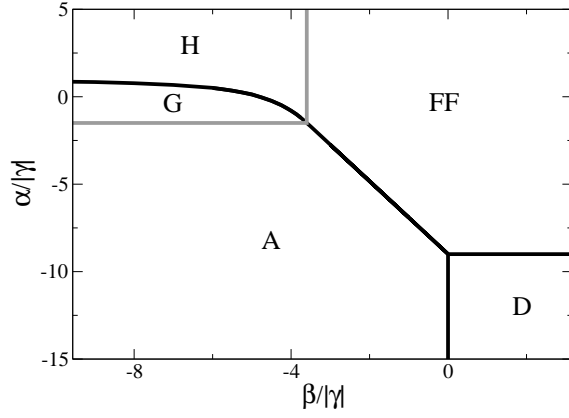


FIG. 2: Phase diagram in zero magnetic field for  $\gamma < 0$ . The solid and grey lines are first and second order boundaries, respectively. The nature of the phases is discussed in Fig. 3.

Phase	$\langle \mathbf{S} \rangle$	Nematic tensor	$\Theta$	$\zeta$
A	0		1	$(1, 0, 0, 0, 0, 1)/\sqrt{2}$
B	0		$0 < \Theta < 1$	$(a, 0, b e^{i\delta}, 0, b e^{i\delta}, 0, a)$
C	$> 0$	$\langle \mathbf{S} \rangle \parallel \mathbf{e}_{2,3}$	$0 < \Theta < 1$	$(a, 0, b, 0, c, 0, d)$
D	0		0	$(\sqrt{2}, 0, 0, i\sqrt{5}, 0, 0, \sqrt{2})/3$
E	0		$0 < \Theta < 1$	$(a, 0, b, 0, c, 0, d)$
F	2		0	$(0, 1, 0, 0, 0, 0, 0)$
FF	3	$\langle \mathbf{S} \rangle \parallel \mathbf{e}_3$	0	$(1, 0, 0, 0, 0, 0, 0)$
G	$> 0$	$\langle \mathbf{S} \rangle \parallel \mathbf{e}_1$	$0 < \Theta < 1$	$(0, a, 0, b, 0, c, 0)$
H	$> 0$	$\langle \mathbf{S} \rangle \parallel \mathbf{e}_3$	0	$(a, 0, 0, 0, 0, b, 0)$

FIG. 3: Phases present at  $p = 0$ .  $a, b, c, d$  and  $\delta$  are real numbers.

magnetization  $\langle \mathbf{S} \rangle$  and nematic tensor  $\mathcal{N}$ . An isotropic  $\mathcal{N}$  ( $\lambda_1 = \lambda_2 = \lambda_3$ ) will be denoted by a sphere. Uniaxial nematics with ( $\lambda_1 = \lambda_2 < \lambda_3$ ) and ( $\lambda_1 < \lambda_2 = \lambda_3$ ) are represented by a long and flat cylinder, with major and minor axis being the symmetry axis of the cylinder respectively. Biaxial nematics with ( $\lambda_1 < \lambda_2 < \lambda_3$ ) are represented as a “brick” with edge lengths given by  $\lambda_a$ . The principal axis  $\hat{\mathbf{e}}_a$  is parallel to the edge with length  $\lambda_a$ . Figure 3 shows the structure of the phases. In particular, (A) *Maximum polar state*: This state has time reversal symmetry, since  $\Theta = 1$ . It is a uniaxial nematic with  $\lambda_3 = 9$ ,  $\lambda_{1,2} = 3/2$ . (B) *Co-linear polar state*: It is a superposition of two polar states  $(1, 0, 0, 0, 0, 0, 1)$  and  $(0, 0, 1, 0, 1, 0, 0)$  with unequal weight and a relative phase. This system is non-magnetic  $\langle \mathbf{S} \rangle = 0$  and yet has broken time reversal symmetry,  $0 < |\Theta| < 1$ . The latter is achieved by the phase angle  $\delta$ , which varies from 1.3 to 1.4 along the Cr-line from bottom to top. The system is uniaxial nematic with  $\lambda_1 < \lambda_2 = \lambda_3$ . (C)

*Biaxial nematic ferromagnet*: The system has a weak spontaneous magnetization  $\langle \mathbf{S} \rangle = M \hat{\mathbf{z}}$ ,  $M = 0.07$  to 0.08, and is a biaxial nematic with either  $\hat{\mathbf{e}}_2$  or  $\hat{\mathbf{e}}_3$  along  $\langle \mathbf{S} \rangle$ . Since  $M$  is small, the contribution of the  $\gamma$  term in eq.(1), (and hence dipolar energy) is a very small contribution to the total energy. This structure is driven largely by the competition between the nematic and the singlet contribution. The boundary separating B and C is  $\tilde{\alpha} = 3|\tilde{\beta}|/(3|\tilde{\beta}| + 2)$ ,  $\tilde{\alpha} = \alpha/\gamma$ ,  $\tilde{\beta} = \beta/\gamma$ . The behaviors of  $\lambda_a$  and  $|\langle \mathbf{S} \rangle|$  are shown in fig.4. The properties of these phases are tabulated in fig.4. The boundary between G and H is  $\tilde{\alpha} = (24\tilde{\beta} + 5\tilde{\beta}^2)/(36 + 24\tilde{\beta} + 5\tilde{\beta}^2)$  [9].

#### V. Phase diagram in non-zero magnetic field:

Figure 5 shows the phase diagram along the Cr-line in figure 1 for  $p \neq 0$  obtained by minimizing eq.(4). It has an intricate structure near  $\alpha = 0$ . All states have non-zero magnetization  $\langle \mathbf{S} \rangle$  along the direction of the magnetic field  $\hat{\mathbf{z}}$ , represented as an arrow. The main features of our results are:

(i) The transition  $A_1 \rightarrow Z_1 \rightarrow G_1$  is a rotation of uniaxial nematic tensor in the  $A_1$  phase (represented as a long cylinder) along its middle principal axis  $\hat{\mathbf{e}}_2$  as one crosses the phase  $Z_1$ , with the rotation angle finally reaching  $90^\circ$  at the  $G_1$  phase. However, in the  $Z_1$  phase,  $\mathcal{N}$  acquires biaxial nematicity, which continues into the  $G_1$  phase. (ii) As  $p \rightarrow 0$ , for  $\alpha/\gamma < -0.372$  and  $\alpha/\gamma > -0.372$ , the states  $\zeta_{A_1}^T$  and  $\zeta_{G_1}^T$  reduce to  $(1, 0, 0, 0, 0, 0, 1)/\sqrt{2}$  and  $(0, \sqrt{3}, 0, \sqrt{10}, 0, \sqrt{3}, 0)/4$  resp., which are related to each other by a  $90^\circ$  rotation about  $\hat{\mathbf{y}}$ . (iii) The transition  $A_1 \rightarrow Z_1 \rightarrow H_1$  is a similar rotation process as in (i) except that the rotational angle is zero when one reaches the  $H_1$  phase. The nematic tensor  $\mathcal{N}$  of  $H_1$  is again uniaxial, except that  $H_1$  has zero singlet amplitude, unlike  $A_1$ . (iv)  $G_1$  and  $G_2$  have similar tensor  $\mathcal{N}$ . There is, however, a jump in  $\Theta$  across their boundary. (v) As the B phase in figure 1 extends into the  $B_1$  phase in finite field  $p$ , its nematic tensor  $\mathcal{N}$  changes from uniaxial to biaxial, merging into the  $C_1$  phase, the finite field extension of C. (vi) Among all phases in

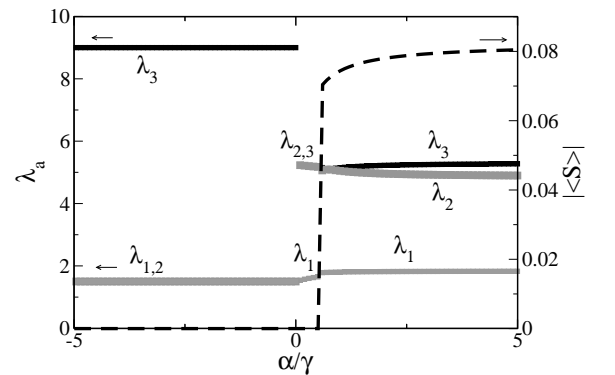


FIG. 4: The eigenvalues  $\lambda_a$  of  $\mathcal{N}$  and the magnetization  $\langle \mathbf{S} \rangle$  along the Cr-line in figure 1.

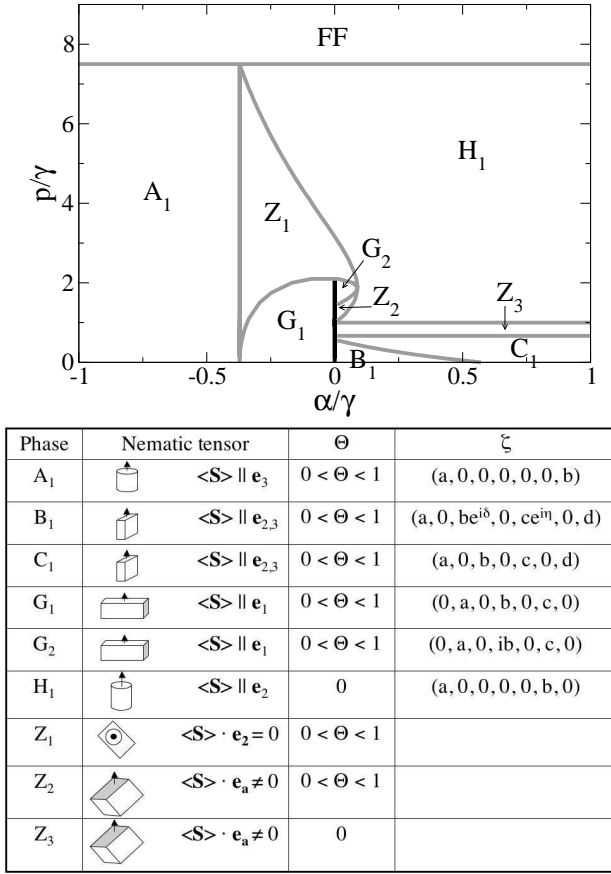


FIG. 5: Top panel: Phase diagram for non-zero magnetic field along the Cr-line in fig.1. The solid and grey lines are first and second order boundaries, respectively. Bottom panel: Explanation of the phases in the diagram. The numbers  $a, b, c, d$  are real. All entries of the wavefunctions for the  $Z_j$  phases are generally non-zero. It is not clear they can be represented in a simple form as the other phases.

finite field,  $Z_1, Z_2$  and  $Z_3$  are the ones where none of their principal axes are aligned with  $\hat{\mathbf{z}}$ . The  $Z_1$  has its middle axis  $\hat{\mathbf{e}}_2 \perp \hat{\mathbf{z}}$ . In both  $Z_2$  and  $Z_3$ , none of the direction cosines  $\hat{\mathbf{e}}_a \cdot \hat{\mathbf{z}}$  vanish. Among these three phases,  $Z_3$  is the only phase that has vanishing singlet amplitude. The phase boundary between  $C_1 - Z_3$  and  $Z_3 - H_1$  are straight lines at  $p/\gamma = 0.667$  and  $1$  resp. (vii) The system becomes a full ferromagnet ( $FF$ ) when  $p/\gamma > 7.5$ . To observe the spinor feature, we then need  $B < B_c$ , where  $B_c = (7.5)\gamma(2\pi\hbar^2 a_B n/M)/(g\mu_B)$ . Using  $g = 2, \gamma = 4.91$ , we have  $B_c = [8.34 \times 10^{-19} n]$ Gauss, where  $n$  is in units of  $\text{cm}^{-3}$ . Thus, with  $n = 5 \times 10^{12}$  to  $10^{14} \text{ cm}^{-3}$ ,  $B_c = 4.2 \times 10^{-6}$  to  $10^{-4}$  Gauss.

**Detection :** Although the ground states of eq.(1) are determined up to an arbitrary rotation about  $\hat{\mathbf{z}}$ , this de-

generacy can be lifted by the anisotropy of a trap through dipole interaction eq.(3). With the principal axes (i.e.  $\{\hat{\mathbf{e}}_a\}$ ) fixed by the magnetic field and the trap, the eigenvalues  $\lambda_a$  can be determined by performing Stern-Gerlach experiments along the axes  $\hat{\mathbf{e}}_a$ .

**Final Remarks:** The realization of quantum spin nematics, especially the biaxial ones, will be an exciting development in both cold atom/condensed matter physics. These are novel states yet to be realized in solid state systems, and biaxial nematics are known to have nonabelian defects. Although reducing the magnetic field to the spinor condensate regime for Cr is a challenging task, screening a field to  $10^{-4}$ Gauss is not outside the reach of current technology. Furthermore, in optical lattice setting, one can further increase the density with each lattice site, making it easier to reach the spinor regime. From the present work, it will not be surprising if spin nematics can also be found in other higher spin Bose gases.

T.L. Ho would like to thank T. Pfau and Marco Fattori for discussions. This work is supported by NASA GRANT-NAG8-1765 and NSF Grant DMR-0426149.

- 
- [1] A. Griesmaier et al., Phys. Rev. Lett. **94**, 160401 (2005).
  - [2] J. Stuhler et al., Phys. Rev. Lett. **95**, 150406 (2005).
  - [3] T.L. Ho, Phys. Rev. Lett. **81**, 742 (1998).
  - [4] While this paper was being prepared, a preprint by L. Santos et al. (cond-mat/0510634) on the same problem appeared. Our results, however, are in complete disagreement. We believe the difference is partly due to their assumption that  $\mathcal{N}$  must be uniaxial along the field direction  $\hat{\mathbf{z}}$  with  $\langle S_x^2 \rangle = \langle S_y^2 \rangle$ ,  $\mathcal{N}_{xy} = \mathcal{N}_{yz} = \mathcal{N}_{zx} = 0$ , which in general need not be true. We also note that having used a functional obtained from the uniaxial assumption, their results  $\psi_{01}$  and  $\psi_{23}$  do not satisfy the uniaxial constraint and have  $\langle \mathbf{S} \rangle \times \hat{\mathbf{z}} \neq 0$ .
  - [5] Using the identities  $1 = P_0 + P_2 + P_4 + P_6$ ,  $\mathbf{S}_1 \cdot \mathbf{S}_2 = -12P_0 - 9P_2 - 2P_4 + 9P_6 = 9 - 21P_0 - 18P_2 - 11P_4$  for a pair of spin-3 bosons with contact interaction, where  $P_S$  is the projection operator for total spin  $S$ , we can trade  $P_6$  and  $P_4$  with a constant and  $\mathbf{S}_1 \cdot \mathbf{S}_2$ .
  - [6] Using  $(\mathbf{S}_1 \cdot \mathbf{S}_2)^2 = 81 + 441P_0 + 324P_2 + 121P_4 = 180 + 210P_0 + 126P_2 - 11\mathbf{S}_1 \cdot \mathbf{S}_2$ , we have  $\sum_M |B_M|^2 = \frac{1}{18} \text{Tr} \mathcal{N}^2 + \frac{7}{12} (\mathbf{S})^2 - \frac{5}{3} |\Theta|^2 - 10$ .
  - [7]  $E_D = \frac{(g\mu_B)^2}{2} \int d\mathbf{r} d\mathbf{r}' n(|bfr)n(\mathbf{r}') \langle \mathbf{S} \rangle_{\mathbf{r}} \langle \mathbf{S} \rangle_{\mathbf{r}'} D_{ij}(\mathbf{r} - \mathbf{r}')$ , where  $g$  is the Lande  $g$ -factor,  $\mu_B$  is the Bohr magneton,  $D_{ij}(\mathbf{R}) = (\delta_{ij} R^2 - 3R_i R_j)/R^5$ , and  $\langle \mathbf{S} \rangle_{\mathbf{r}} = \zeta_{\mu}^*(\mathbf{r}) \mathbf{S}_{\mu\nu} \zeta_{\nu}(\mathbf{r})$ .
  - [8] C. V. Ciobanu et al., Phys. Rev. A **61**, 033607 (2000).
  - [9] For  $\beta/|\gamma| < -6$  the H phase is degenerate with the I phase, which is a uniaxial nematic with  $\langle \mathbf{S} \rangle \parallel \mathbf{e}_1$ .